

Spin-transfer-driven nano-oscillators are equivalent to parametric resonators

Alejandro O. León* and Marcel G. Clerc†

Departamento de Física, Facultad de Ciencias Físicas y Matemáticas, Universidad de Chile, Casilla 487-3, Santiago, Chile

(Received 28 April 2014; revised manuscript received 19 December 2014; published 12 January 2015)

The equivalence between different physical systems permits us to transfer knowledge between them and to characterize the universal nature of their dynamics. We demonstrate that a nanopillar driven by a spin-transfer torque is equivalent to a rotating magnetic plate, which permits us to consider the nanopillar as a macroscopic system under a time-modulated injection of energy, that is, a simple parametric resonator. This equivalence allows us to characterize the phases diagram and to predict magnetic states and dynamical behaviors, such as solitons, stationary textures, and oscillatory localized states, among others. Numerical simulations confirm these predictions.

DOI: [10.1103/PhysRevB.91.014411](https://doi.org/10.1103/PhysRevB.91.014411)

PACS number(s): 75.76.+j, 75.75.Jn, 75.78.-n

I. INTRODUCTION

Current-driven magnetization dynamics have attracted much attention in recent years because of both the rich phenomenology that emerges and the promising applications in memory technology [1]. A remarkable example occurs when a direct spin-polarized current applies a torque to nanoscale ferromagnets, an effect known as spin-transfer torque [2,3]. This effect has been confirmed experimentally [4–9], and, in particular, the observation of magnetization reversal caused by spin-transfer torques was reported in Refs. [6,7,10,11]. Spin-transfer effects are usually studied in the metallic multilayer nanopillar, or spin-valve, depicted in Fig. 1(a), where two magnetic films (light layers), the *free* and the *fixed*, are separated by a nonmagnetic spacer (darker layer). In such a nanopillar, an electric current J applied through the spin-valve transfers spin angular momentum from the film with *fixed* magnetization to the *free* ferromagnetic layer.

When the direct current overcomes a critical value, the spin-transfer torque destabilizes the state in which both magnetizations point parallel, and the free magnetization switches or precesses in the microwave-frequency domain. Most scientific efforts have focused on this regime, in which the free magnetization behaves as a self-oscillator with negative damping [12]. Another interesting case is when there is an external field that disfavors the parallel state and the spin-polarized current favors it; under this regime, it is expected that the system will generate complex dynamics as a result of both opposing effects.

The aim of this article is to show that nanopillars under the effect of a spin-polarized direct electric current exhibit the same dynamics present in systems with a time-modulated injection of energy, known as parametric systems [13]. Parametric systems oscillate at half of the forcing frequency, a phenomenon known as parametric resonance. Examples of parametric systems include a layer of water oscillating vertically [14], localized structures in nonlinear lattices [15], light pulses in optical fibers [16], optical parametric oscillators [17], and easy-plane ferromagnetic materials exposed to an oscillatory magnetic field [18].

To understand the parametric nature of the spin-transfer-driven nanopillars, we put in evidence that this system is equivalent to a simple rotating magnetic plate subjected to a constant magnetic field applied in the rotation direction [see Fig. 1(b)], where the electric current intensity on the nanopillar corresponds to the angular velocity in the equivalent rotational system. We analytically show that the magnetization dynamic of a nanopillar under the effect of a spin-transfer torque is well described by the *parametrically driven, damped nonlinear Schrödinger equation* (PDNLS). This equation is the paradigmatic model of parametric systems with small injection and dissipation of energy [19]. Based on this model we predict that the spin-transfer torque generates equilibria, solitons, oscillons, patterns, propagative walls between symmetric periodic structures, and complex behaviors, among others. Numerical simulations of the Landau-Lifshitz-Gilbert equation confirm these theoretical predictions.

The manuscript is organized as follows. In the next section we present the nanopillar and the equation of motion of an homogeneous free magnetization. In Sec. III, we analyze the relation between the nanopillar and parametric systems. In Sec. IV we explore the inhomogeneous dynamics predicted by the parametric nature of the spin-transfer torque effect at dominant order. Finally, in Sec. V, we give the conclusions and remarks.

II. MACROSPIN DYNAMICS OF THE FREE LAYER

Consider a nanopillar device, with fixed layer magnetization \mathbf{M}_0 along the positive x axis as depicted by Fig. 1; this ferromagnet has a large magnetocrystalline anisotropy or it is thicker than the free layer, and therefore it acts as a polarizer for the electric current. Let us assume that the free layer is a single-domain magnet, that is, the magnetization rotates uniformly $\mathbf{m}(\mathbf{r}, t) = \mathbf{m}(t)$.

Hereafter, we work with the following adimensionalization: The magnetization of the free layer $\mathbf{M} \rightarrow M_s \mathbf{m}$ and the external field $\mathbf{H}_a \rightarrow M_s \mathbf{h}_a$ are normalized by the saturation magnetization M_s ; moreover, the time $t \rightarrow \gamma M_s t$ is written in terms of the gyromagnetic constant γ and M_s . For instance, in a cobalt layer of 3 nm thickness, $M_s \simeq 1.4 \times 10^6$ A/m, and the characteristic time scale is $(\gamma M_s)^{-1} \simeq 3.2$ ps [20].

*aoleon@dfi.uchile.cl

†marcel@dfi.uchile.cl

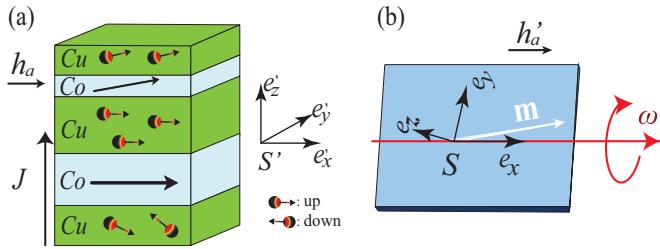


FIG. 1. (Color online) Equivalent physical systems. (a) Schematic representation of the spin-transfer torque nano-oscillator setup. The light (blue) and dark (green) layers represent magnetic and nonmagnetic metal films, respectively. J and h_a are the electric current through the spin-valve and the external magnetic field, both effects are parallel to the easy axes of the ferromagnetic layer under study. \mathbf{M}_0 stands for the magnetization of the fixed layer. (b) Rotating magnetic plate with an easy axis in the rotation direction, subjected to a constant magnetic field, \mathbf{h}'_a .

When the free magnetization is homogeneous, the normalized magnetic energy per unit of volume is [20]

$$\frac{E}{\mu_0 M_s^2} = -\mathbf{m} \cdot \mathbf{h}_a - \frac{1}{2} \beta_x m_x^2 + \frac{1}{2} \beta_z m_z^2, \quad (1)$$

and the external magnetic field $\mathbf{h}_a = h_a \mathbf{e}_x$ points along the x axis (see Fig. 1). The coefficients β_x and β_z are combinations of the normalized anisotropy and demagnetization constants with respect to the appropriate axes, where β_x (β_z) favors (disfavors) the free magnetization in the x axis (z axis).

The dynamic of the magnetization of the free layer is described by the dimensionless Landau-Lifshitz-Gilbert equation (LLG) with an extra term that accounts for the spin-transfer torque [2,6,7,20,21],

$$\frac{d\mathbf{m}}{dt} = -\mathbf{m} \times \mathbf{h}_{\text{eff}} + \alpha \mathbf{m} \times \frac{d\mathbf{m}}{dt} + g \mathbf{m} \times (\mathbf{m} \times \mathbf{e}_x). \quad (2)$$

The first term of the right-hand side of Eq. (2) accounts for the conservative precessions generated by the effective field,

$$\mathbf{h}_{\text{eff}} \equiv -\frac{1}{\mu_0 M_s^2} \frac{\delta E}{\delta \mathbf{m}} = (h_a + \beta_x m_x) \mathbf{e}_x - \beta_z m_z \mathbf{e}_z. \quad (3)$$

The second and third terms of Eq. (2) are the phenomenological Gilbert damping and the spin-transfer torque respectively. The dimensionless prefactor g is given by [11] $g \equiv \mathcal{P}(m_x)(\hbar/2)(J/d|e|)(1/\mu_0 M_s^2)$, and \mathcal{P} describes the electron polarization at the interface between the magnet and the spacer, J the current density of electrons, d the thickness of the layer, and $e < 0$ the electric charge. The current density of electrons J and the parameter g are negative when the electrons flow from the fixed to the free layer. There are different expressions for the polarization $\mathcal{P}(m_x)$ in the literature [2,22–25]. For certain types of nanopillars, a better agreement with experimental observations is obtained if $\mathcal{P}(m_x)$ is constant, see Refs. [24,26,27] for more details.

The dynamics of LLG are characterized by the conservation of the magnetization magnitude $\|\mathbf{m}\| = 1$, since \mathbf{m} and $d\mathbf{m}/dt$ are perpendicular. The LLG model, Eq. (2), admits two natural equilibria $\mathbf{m} = \pm \mathbf{e}_x$, which represent a free magnetization that is parallel (+) or antiparallel (–) to the fixed magnetization \mathbf{M}_0 [see Fig. 1(a)]. Both states correspond to extrema of the

free energy E . We will concentrate on the equilibrium $\mathbf{m} = \mathbf{e}_x$; nevertheless due to the symmetries of the LLG equation, the same results hold for $\mathbf{m} = -\mathbf{e}_x$ when replacing (g, h_a) with $(-g, -h_a)$.

III. EQUIVALENT PHYSICAL SYSTEMS

Let us consider a rotating magnetic plane with angular velocity $\Omega = \Omega_0 \mathbf{e}_x$ and an easy axis in the rotation direction, subjected to a constant magnetic field applied in the rotation direction $\mathbf{h}'_a = (h_a + \Omega_0) \mathbf{e}_x$ [see Fig. 1(b)].

This rotating ferromagnet can be described in both the co-movil frame S , defined by the vectors $\{\mathbf{e}_x, \mathbf{e}_y, \mathbf{e}_z\}$, or in the inertial frame S' , defined by $\{\mathbf{e}'_x, \mathbf{e}'_y, \mathbf{e}'_z\}$. Note that the ferromagnetic easy axis is described by the same vector in the both frames ($\mathbf{e}'_x = \mathbf{e}_x$); nevertheless, unit vectors $\mathbf{e}_y(t) = \cos(\Omega_0 t) \mathbf{e}'_y + \sin(\Omega_0 t) \mathbf{e}'_z$ and $\mathbf{e}_z(t) = -\sin(\Omega_0 t) \mathbf{e}'_y + \cos(\Omega_0 t) \mathbf{e}'_z$ rotate together with the magnetic plate [see Fig. 1(b)]. In the co-movil system the normalized magnetic energy will be the same of Eq. (1); however, in the inertial frame the energy depends explicitly in time,

$$\begin{aligned} \frac{E'}{\mu_0 M_s^2} = & -\mathbf{m} \cdot \mathbf{h}'_a - \frac{1}{2} \beta_x m_x'^2 + \frac{1}{2} \beta'_{zz}(t) m_z'^2 \\ & + \frac{1}{2} \beta'_{yy}(t) m_y'^2 + \frac{1}{2} \beta'_{yz}(t) m'_y m'_z, \end{aligned} \quad (4)$$

where the time varying coefficients $\beta'_{zz} = \beta_z [1 + \cos(2\Omega_0 t)]/2$, $\beta'_{yy} = \beta_z [1 - \cos(2\Omega_0 t)]/2$, and $\beta'_{yz} = -\beta_z \sin(2\Omega_0 t)$ act as a parametric forcing. Note that the frequency of the forcing is twice the frequency of the rotations. Therefore, this system presents a subharmonic parametric resonance [13].

The dynamics of the magnetic plane in the inertial frame S' is described by the Landau-Lifshitz-Gilbert equation

$$\left. \frac{d\mathbf{m}}{dt} \right|_{S'} = -\mathbf{m} \times \mathbf{h}'_{\text{eff}}(t) + \alpha \mathbf{m} \times \left. \frac{d\mathbf{m}}{dt} \right|_{S'}, \quad (5)$$

where $\mathbf{h}'_{\text{eff}} = -(1/\mu_0 M_s^2)(\delta E'/\delta \mathbf{m})$. Let us now write the Eq. (5) in the noninertial frame S , where the time derivative operator in the rotating system takes the form $\partial_t|_{S'} = \partial_t|_S + \Omega \times$ [13], thus the dynamics of the rotating magnetic plate in the noninertial frame S reads

$$\begin{aligned} \left. \frac{d\mathbf{m}}{dt} \right|_S = & -\mathbf{m} \times \mathbf{h}_{\text{eff}} + \alpha \mathbf{m} \times \left. \frac{d\mathbf{m}}{dt} \right|_S \\ & - \alpha \Omega_0 \mathbf{m} \times (\mathbf{m} \times \mathbf{e}_x), \end{aligned} \quad (6)$$

where the effective field \mathbf{h}_{eff} is the same of formula (3). Therefore, the dynamics of the rotating magnetic plate in the noninertial frame S , Eq. (6), is a time-independent equation, which is equivalent to the dynamics of a nanopillar under the effect of a spin-transfer torque generated by a uniform electric current, Eq. (2). In this equivalence, the intensity of the spin-transfer effect on the nanopillar g corresponds to the angular velocity by the dissipation parameter, $-\alpha \Omega_0$. Indeed, the two physical systems depicted in Fig. 1 are equivalent. In the next sections, we will apply the well-known understanding on parametric systems to the nano-oscillator.

**Parametrically driven damped nonlinear
Schrödinger equation**

To obtain a simple model that permits analytical calculations around the parallel state, we use the following stereographic representation [28]:

$$\psi(\mathbf{r}, t) = \frac{m_y + im_z}{1 + m_x}, \quad (7)$$

where ψ is a complex field. This representation corresponds to consider an equatorial plane intersecting the magnetization unit sphere. The magnetization components are related with the complex field by $m_x = (1 - |\psi|^2)/(1 + |\psi|^2)$, $m_y = (\psi + \bar{\psi})/(1 + |\psi|^2)$, and $m_z = (i(\bar{\psi} - \psi))/(1 + |\psi|^2)$, where $\bar{\psi}$ stands for the complex conjugate of ψ . Notice that the parallel state $\mathbf{m} = \mathbf{e}_x$ is mapped to the origin of the ψ plane. The LLG, Eq. (2) or Eq. (6), takes the following form:

$$(i + \alpha) \frac{d\psi}{dt} = (ig - h_a) \psi - \frac{\beta_z}{2} (\psi - \bar{\psi}) \frac{1 + \psi^2}{1 + |\psi|^2} - \beta_x \psi \frac{1 - |\psi|^2}{1 + |\psi|^2}. \quad (8)$$

This is a complex Ginzburg-Landau-type equation, which describes the envelope of a nonlinear dissipative oscillator.

An advantage of the stereographic representation is to guarantee the magnetization normalization and to consider the appropriate degrees of freedom. Notice that the switching dynamic between parallel and antiparallel state is not well described, since the antiparallel state is represented by infinity [28]. This kind of dynamics is not considered in the present work. To grasp the dynamical behavior exhibited by the previous model, let us consider that the complex amplitude is small and that the parameters $\alpha, \beta_z/2$ are also small. Introducing the renormalized amplitude $A(\mathbf{r}, t) = \psi(\mathbf{r}, t)e^{i\pi/4} \sqrt{2\beta_x + \beta_z}$, after straightforward calculations, Eq. (8) is approximated at dominant order by

$$\frac{dA}{dt} = -ivA - i|A|^2A - \mu A + \gamma \bar{A}, \quad (9)$$

where $\mu \equiv -g - \alpha v$, $v \equiv -h_a - (\beta_x + \beta_z/2)$, and $\gamma \equiv \beta_z/2$. Thus under the above assumptions the nanopillar resonator is described by Eq. (9), which is known as the PDNLS equation without space. This model has been used to describe parametric resonators [13].

The coefficient γ is the intensity of the forcing in usual parametric systems. For instance, it is proportional to the amplitude of the oscillation in vibrated media or the intensity of time-dependent external fields. In the case of the nanopillar $\gamma = \beta_z/2$ is not a control parameter. In the context of the PDNLS amplitude equation γ breaks the phase invariance, i.e., $A \rightarrow Ae^{i\phi_0}$. A change of variables of the form $A = Be^{i\omega t}$ (rotating frame) permits us to restore the explicit time-dependent forcing,

$$\frac{dB}{dt} = -i(v + \omega)B - i|B|^2B - \mu B + \gamma e^{-2i\omega t} \bar{B}. \quad (10)$$

Moreover, in this representation the parametric nature of the PDNLS equation is evident. The parameter $\mu > 0$ accounts for dissipation in parametric systems and it models radiation, viscosity, and friction, depending on the particular physical

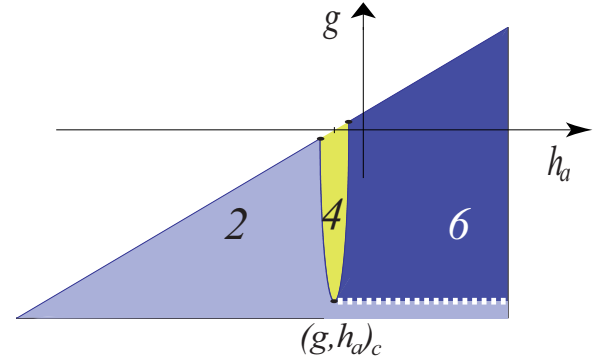


FIG. 2. (Color online) Bifurcation diagram of the parallel state $\mathbf{m} = \mathbf{e}_x$, in the dark zone $\mathbf{m} = \mathbf{e}_x$, is stable. The elliptical-like light zone delimited by $g^2 + [h_a - (\beta_x + \beta_z/2)]^2 = \beta_z^2/4$ is known as Arnold's tongue. In this region there are four equilibria and the parallel state is unstable. On the left of Arnold's tongue and above the segmented curve $g = -\beta_z/2$ there are six equilibria.

context. In our case, this dissipation is the combination of the Gilbert damping and the spin-polarized current. Finally, the detuning v accounts for the deviation from a half of the forcing frequency. In the case of the nanopillar, v is controlled by the external field.

To obtain Eq. (9) we have assumed that $\alpha, \beta_z/2 \ll 1$ and that the amplitude is a slowly varying amplitude ($|A| \ll 1$), that is, we have the scaling $|A|^2 \sim v \sim \mu \sim \gamma \sim \partial_t \ll 1$. Notwithstanding, the model, Eq. (9), is qualitatively valid outside this limit.

The parallel state $A = 0$ is always a solution of Eq. (9). Decomposing the amplitude into its real and imaginary parts $A(t) = u(t) + iv(t)$ and linearizing around them, we have

$$\frac{d}{dt} \begin{pmatrix} u \\ v \end{pmatrix} = \begin{bmatrix} \gamma - \mu & v \\ -v & -(\gamma + \mu) \end{bmatrix} \begin{pmatrix} u \\ v \end{pmatrix}. \quad (11)$$

Imposing a solution of the form $(u, v) \sim e^{\lambda \pm t} (u_0, v_0)$, we obtain the growth rate relation $\lambda_{\pm} = -\mu \pm \sqrt{\gamma^2 - v^2}$. The stability condition, which corresponds to $\text{Re}(\lambda_{\pm}) < 0$ is shown in dark areas in Fig. 2. The elliptical-like light zone of Fig. 2 is known as Arnold's tongue in the context of parametric systems, and it accounts for the destabilization of the parallel state for $\mu^2 + v^2 = \gamma^2$. The exact curve of the Arnold's tongue in terms of the original parameters can be obtained from the LLG equation without neglecting α , that is, $g^2 + [h_a - (\beta_x + \beta_z/2)]^2 = \beta_z^2/4$. Inside the Arnold's tongue this model has also the equilibria

$$A_{\pm} = \pm \left(1 - i \sqrt{\frac{\gamma - \mu}{\gamma + \mu}} \right) \sqrt{\frac{\gamma + \mu}{2\gamma} (\sqrt{\gamma^2 - \mu^2} - v)}. \quad (12)$$

In this region there are four equilibria (see Fig. 2); they are the parallel state $A = 0$ (equivalently $\mathbf{m} = \mathbf{e}_x$), the antiparallel state ($\mathbf{m} = -\mathbf{e}_x$) and A_{\pm} . Crossing the curve of the Arnold's tongue for positive detuning $\sqrt{\gamma^2 - \mu^2} = v > 0$, the A_{\pm} states and $A = 0$ collide together through a pitchfork bifurcation. For greater values of the detuning parameter v , only the parallel and antiparallel states exist.

For negative detuning and $\gamma > \mu$ (above the dashed curve in Fig. 2), and outside Arnold's tongue $\sqrt{\gamma^2 - \mu^2} < |\nu|$, the A_{\pm} states exist and are stable. Since the $A = 0$ equilibrium is also stable in this region, it is necessary to have other two states A'_{\pm} that separate them in the phases space which have the form

$$A'_{\pm} = \pm \left(1 + i \sqrt{\frac{\gamma - \mu}{\gamma + \mu}} \right) \sqrt{\frac{\gamma + \mu}{2\gamma} (-\sqrt{\gamma^2 - \mu^2} - \nu)}. \quad (13)$$

In this region (the darkened area in Fig. 2), there are six equilibria. Thus the PDNLS equation describes the homogeneous stationary solutions which have been studied in the context of the nano-oscillator [20,29].

When $g \leq -\alpha\nu$ the coefficient that rules the dissipation becomes negative, and the magnetization oscillates and moves away from the parallel state. This instability is known as the Andronov-Hopf bifurcation [30]. When it does not saturate the magnetization switches to the antiparallel state or reaches another stationary equilibrium. Precessions or self-oscillations emerge when this instability saturates. In the past, this regime has been extensively studied experimentally and theoretically in the context of the spin-transfer torque resonator [8,10,12]. This instability does not occur in usual parametric systems since the dissipation coefficient is always positive $\mu > 0$.

In brief, the nanopillars driven by a spin-transfer torque effect are equivalent to parametric systems, and then they are well described by the paradigmatic model for parametric systems, the PDNLS equation without space. We will see in the next section the predictions of this model for the nanopillar in the case of a variable magnetization.

IV. GENERALIZATION TO AN INHOMOGENEOUS MAGNETIZATION DYNAMICS

The macrospin approximation permits us to understand several features of the magnetization dynamics driven with spin torque, but, even so, this approximation is not completely valid because in general both the precession and magnetic reversion are inhomogeneous [31]. There are several approaches to study the nonuniform magnetization dynamics; nevertheless, we use here a minimal model with a ferromagnetic exchange torque as the dominant space-dependent coupling in order to understand the emergence of a rich spatiotemporal dynamics.

In the case of an inhomogeneous magnetization $\mathbf{m}(\mathbf{r}, t)$, which corresponds to a spatial extension of the nano-oscillator, the magnetic energy $E = \mu_0 M_s^2 \int \epsilon dx dy$ of the free layer is the integral of the following dimensionless density of energy [20]:

$$\epsilon = -\mathbf{m} \cdot \mathbf{h}_a - \frac{1}{2} \beta_x m_x^2 + \frac{1}{2} \beta_z m_z^2 + \frac{1}{2} |\nabla \mathbf{m}|^2, \quad (14)$$

where $\{x, y\}$ stands for the spatial coordinates of the free layer. The spatial coordinates have been dimensionless $\mathbf{r} \rightarrow l_{\text{ex}} \mathbf{r}$ in terms of the exchange length $l_{\text{ex}} \equiv \sqrt{2A/(\mu_0 M_s^2)}$, where A is the exchange coupling in the ferromagnet. The gradient operator is defined on the plane of the film as $\nabla \equiv \mathbf{e}_x \partial_x + \mathbf{e}_y \partial_y$. The β_x and β_z coefficients account for both the easy axis and the demagnetization in the thin-film approximation [20]. In this approximation, the contribution of the demagnetization effect to the magnetic energy density is local, and the shape of

the thin film is taken into account by the Neumann boundary condition for the magnetization.

The LLG equation and the effective field are

$$\frac{\partial \mathbf{m}}{\partial t} = -\mathbf{m} \times \mathbf{h}_{\text{eff}} + \alpha \mathbf{m} \times \frac{\partial \mathbf{m}}{\partial t} + g \mathbf{m} \times (\mathbf{m} \times \mathbf{e}_x), \quad (15)$$

$$\mathbf{h}_{\text{eff}} \equiv -\frac{1}{\mu_0 M_s^2} \frac{\delta E}{\delta \mathbf{m}} = (h_a + \beta_x m_x) \mathbf{e}_x - \beta_z m_z \mathbf{e}_z + \nabla^2 \mathbf{m}. \quad (16)$$

Notice that gradients come from the ferromagnetic exchange energy, and then the spatial derivatives must be written in terms of the coordinates that label the sample, even if it rotates. Then the equation of the magnetization of the rotating plate in its co-movil frame is Eq. (6) with an extra term for the spatial dependence,

$$\left. \frac{\partial \mathbf{m}}{\partial t} \right|_S = -\mathbf{m} \times \mathbf{h}_{\text{eff}} + \alpha \mathbf{m} \times \left. \frac{\partial \mathbf{m}}{\partial t} \right|_S - \alpha \Omega_0 \mathbf{m} \times (\mathbf{m} \times \mathbf{e}_x), \quad (17)$$

where $\mathbf{h}_{\text{eff}} = (h_a + \beta_x m_x) \mathbf{e}_x - \beta_z m_z \mathbf{e}_z + \nabla^2 \mathbf{m}$ and the $\nabla \equiv \mathbf{e}_x \partial_x + \mathbf{e}_y \partial_y$ operator is defined on the co-movil plane spanned by $(\mathbf{e}_x, \mathbf{e}_y)$. Thus the spatial dependence of \mathbf{m} does not change the equivalence between the nanopillar and the rotating magnet presented in Sec. III. Using the same change of variable of Eq. (7), the LLG Eq. (15) reads

$$(i + \alpha) \partial_t \psi = (ig - h_a) \psi - \frac{\beta_z}{2} (\psi - \bar{\psi}) \frac{1 + \psi^2}{1 + |\psi|^2} - \beta_x \psi \frac{1 - |\psi|^2}{1 + |\psi|^2} + \nabla^2 \psi - 2 \frac{\bar{\psi}}{1 + |\psi|^2} (\nabla \psi)^2, \quad (18)$$

which describes the envelope of coupled nonlinear oscillators. Due to the complexity of this equation, we will consider a simple limit, which permits us to grasp its dynamics. Using the small amplitude that varies slowly in space $A(\mathbf{r}, t) = \psi(\mathbf{r}, t) e^{i\pi/4} \sqrt{2\beta_x + \beta_z}$, we obtain

$$\partial_t A = -i\nu A - i|A|^2 A - i\nabla^2 A - \mu A + \gamma \bar{A}, \quad (19)$$

which is the PDNLS model. The extra term with spatial derivatives describes dispersion.

Parametric textures for nanopillars

The above model, Eq. (19) has been extensively used to study the pattern formation; in particular, this model exhibits solitons, oscillons, periodic textures, and complex behaviors, among others. To verify these predictions, we compare them with the numerical solutions of Eq. (2) in two geometrical configurations. The first is a one-dimensional free layer, that is, a nanopillar for which $\mathbf{m}(\mathbf{r}, t) \approx \mathbf{m}(x, t)$, and the second is a two-dimensional nanopillar with a square cross section. Different transversal lengths are used in simulations, all of them displaying the same qualitative aspects of the solutions. The simulations are conducted using a fifth-order Runge-Kutta algorithm with a constant step size for time integration and finite differences for spatial discretization. The spatial differential operators are approximated with centered schemes

of order 6 and specular (Neumann) boundary conditions are used.

1. Dissipative solitons

Analytical solutions for the dissipative soliton are known in one dimension [18,19,32]. In two dimensions dissipative solitons are observed, however, without analytical expressions. From this result and using the stereographic change of variable, we find the following analytical form for magnetic dissipative solitons in one dimension:

$$m_x = \frac{2\beta_x + \beta_z - R(x)^2}{2\beta_x + \beta_z + R(x)^2},$$

$$\begin{pmatrix} m_y \\ m_z \end{pmatrix} = \frac{2R(x)\sqrt{2\beta_x + \beta_z}}{2\beta_x + \beta_z + R(x)^2} \begin{pmatrix} \cos \varphi_0 \\ \sin \varphi_0 \end{pmatrix}, \quad (20)$$

with $\sin(2\varphi_0) \equiv 2g/\beta_z$, $R \equiv \sqrt{2\delta} \operatorname{sech}[\sqrt{\delta}(x - x_0)]$, and $\delta \equiv h_a + \beta_x + \beta_z/2 + \sqrt{(\beta_z/2)^2 - g^2}$. The width of the soliton is controlled by the external field. The typical sizes are about $10l_{\text{ex}}$.

Figure 3(a) shows the analytical results compared with numerical simulations of the LLG equation, which presents a quite good agreement for small amplitude solitons, i.e., for $\delta \ll 1$. Furthermore, Fig. 3(b) illustrates the dissipative solitons observed numerically in two dimensions. We note that these solitons are well described by a hyperbolic secant function, which was obtained using variational methods [33].

Dissipative solitons are observed in the region of parameter space bounded by $\beta_z^2/2 - (|h_a| - (\beta_x + \beta_z/2))^2 = g^2$ and $\beta_z/2 = |g|$. This region is analytically inferred from the amplitude Eq. (19). Figure 4 shows the respective phase

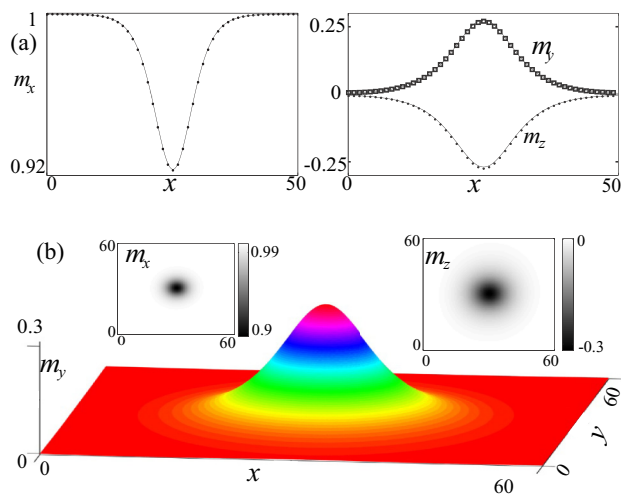


FIG. 3. (Color online) Dissipative solitons in one- and two-dimensional nanopillars (with a square cross section) with $\beta_x = 0.5$, $\beta_z = 1$, and $\alpha = 0.05$. (a) One-dimensional soliton for $g = -0.4999$, $h_a = -0.97$; the points account for the numerical integration of the LLG equation and the line accounts for the analytical solution given by Eq. (20). (b) Soliton in two-dimensions, $g = -0.49995$, $h_a = -0.99$; the three-dimensional plot shows the profile of the component m_y , while the insets show the m_x and the m_z components.

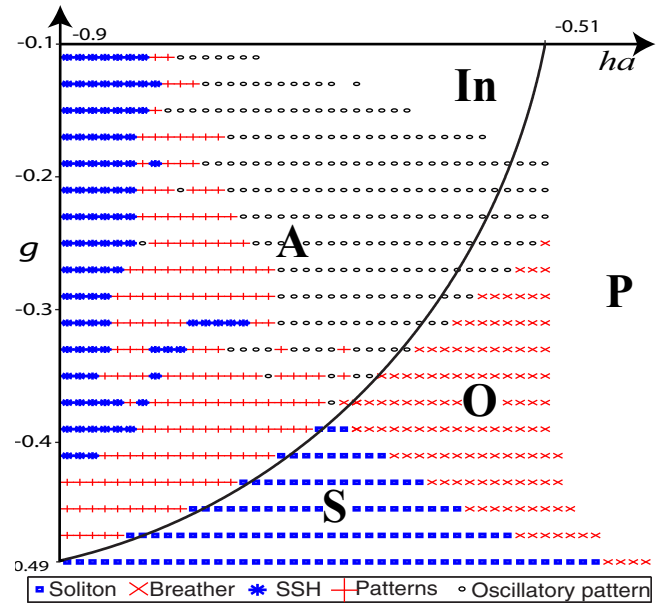


FIG. 4. (Color online) Phase diagram of LLG model, Eq. (2). “S-region” represents solitons region, “O-region” stands for breather solitons (oscillons) region, and “A-region” is the Arnold’s tongue. The In-region accounts for inhomogeneous dynamical states far from the parallel configuration. In the zone P, only the parallel state is observed.

diagram of the LLG equation, and the region of dissipative solitons is denoted by “S-region.”

Increasing the difference between injection and dissipation, $\gamma - \mu$, dissipative solitons undergo an Andronov-Hopf bifurcation, generating oscillatory localized states or breather solitons characterized by exhibiting shoulders in the amplitude profile [34]. Figure 5 illustrates this kind of solution. Similar solutions have also been reported in a magnetic wire forced by a transversal uniform and oscillatory magnetic field [35],

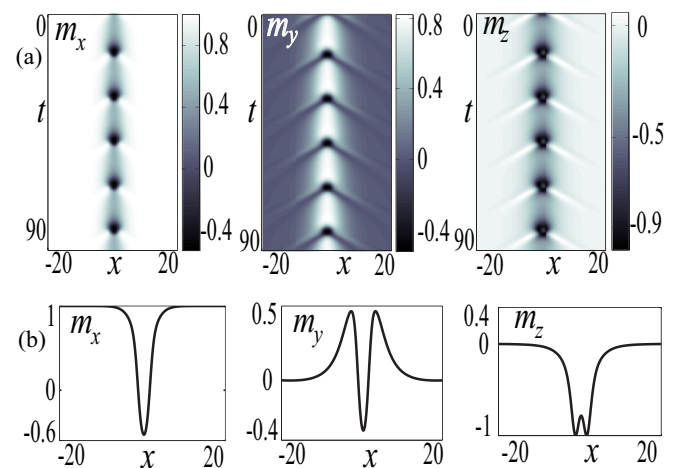


FIG. 5. (Color online) Breather or oscillon solution for $g = -0.33$, $h_a = -0.51$. (a) The spatiotemporal diagram. (b) The magnetization components at the time for which m_x reaches its minimal position. Typical oscillation periods are about $\Delta t \approx 16(\gamma M_s)^{-1}$, which is about $\Delta t \approx 51$ ps for a 3-nm-thick cobalt free layer.

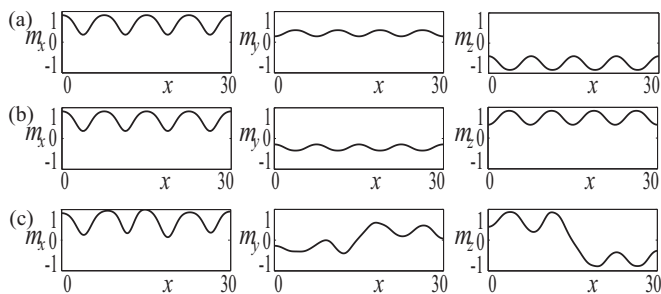


FIG. 6. Dissipative structures for $g = -0.37$, $h_a = -0.75$, inside the Arnold's tongue. [(a) and (b)] Pattern states. (c) Kink solution, this domain wall is a slowly moving front connecting the (a) and (b) patterns.

which corresponds to a parametric system. These oscillatory solutions are observed in the O-region of the bifurcation diagram shown in Fig. 4. Notice that, for spin-transfer torques that favor the parallel state, the nanopillar can also behave as a nano-oscillator.

2. Pattern states

Let us introduce the A-region of the bifurcation diagram (cf. Fig. 4), which is circumscribed by the curve $\beta_z^2/2 - [|h_a| - (\beta_x + \beta_z/2)]^2 = g^2$ in the Arnold's tongue. Inside this region the quiescent state $A = 0$ is unstable, giving rise to a nonzero uniform state and stationary and oscillatory patterns. Figures 6(a) and 6(b) show stable stationary patterns that exist inside the Arnold's tongue, and Fig. 6(c) shows a propagative wall that connects the patterns. In addition, the PDNLS model is characterized by exhibiting supercritical patterns at $\gamma = \mu$ ($\beta_z/2 = |g|$), growing with a power law $1/4$ as a function of the bifurcation parameter [36]. Recently, such dissipative structures induced by spin-transfer torques in nanopillars have been characterized numerically and theoretically [37], where the spatial textures emerge from a spatial supercritical quintic bifurcation. In one spatial dimension, the magnetic patterns read at dominant order by

$$\begin{pmatrix} m_y \\ m_z \end{pmatrix} \approx 2 \left[\frac{4\beta_z(g - g_c)}{(6\beta_x + 3\beta_z - 2k_c^2)^2} \right]^{1/4} \begin{pmatrix} \cos(k_c x) \\ -\cos(k_c x) \end{pmatrix}, \quad (21)$$

and $m_x \approx 1 - (m_y^2 + m_z^2)/2$. Figure 7 shows a pattern solution. The wavelength of the periodic structures, $2\pi/k_c = 2\pi/\sqrt{-h_a - \beta_x - \beta_z}$, is controlled by the external field $h_a < 0$. In two spatial dimensions the system shows the emergence of stripe patterns or superlattices at the onset of bifurcation [37]. The phases diagram of the textures is controlled by a single parameter that accounts for the competition between the external magnetic field, anisotropy, exchange, and the critical spin-polarized current. When the anisotropy is dominant over the external field the system exhibits striped patterns [Fig. 7(b)]; however, when the external field drives the dynamics, the system presents superlattice [Figs. 7(c) and 7(d)] as stable equilibria. Indeed, external fields pointing against the near parallel states favor the formation of more sophisticated spatial textures. Since the electric resistance $R[\mathbf{M}_0 \cdot \mathbf{m}]$ of the nanopillar depends on the relative orientation [31] of the fixed \mathbf{M}_0 and free \mathbf{m} layers, and $\mathbf{M}_0 \cdot \mathbf{m} = m_x \approx 1 - (m_y^2 + m_z^2)/2$

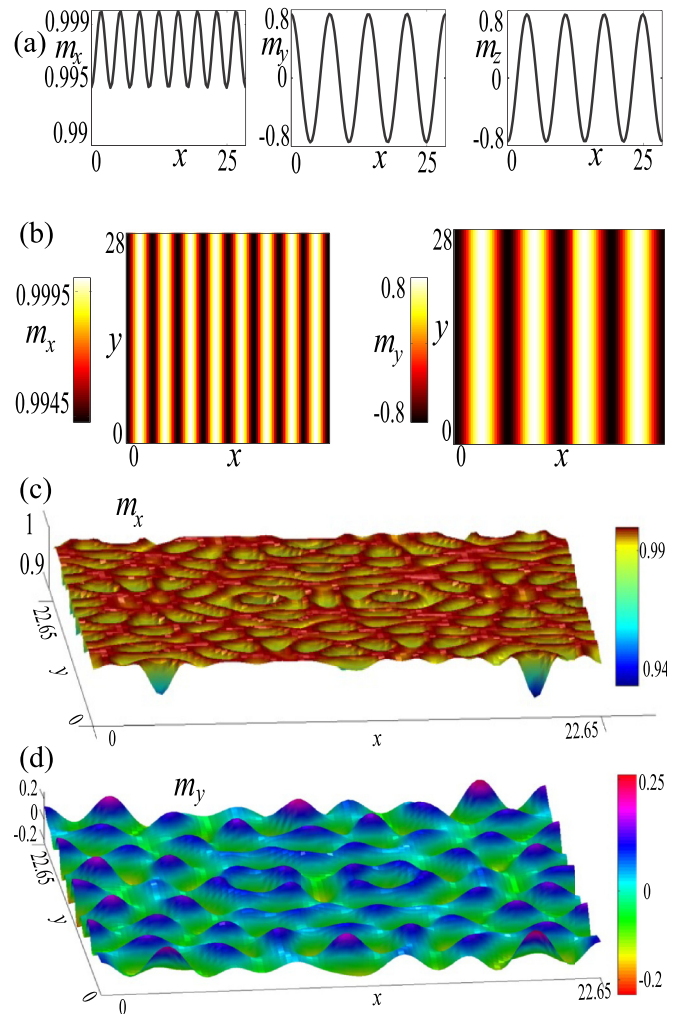


FIG. 7. (Color online) Patterns induced by the spin-polarized current. (a) One-dimensional state for $g = -0.49999$, $h_a = -1.8$, as predicted by Eq. (21), $m_y \approx -m_z$. Notice that the norm conservation implies that $m_x \approx 1 - 0.5(m_y^2 + m_z^2)$ oscillates with a half of the wavelength of the other two components. (b) Bidimensional pattern for the same parameters used in (a), and the component m_z (not shown) is the negative of m_y . (c) The magnetization component m_x for a superlattice pattern obtained with $g = -0.4999$, and $h_a = -6$. (d) The component m_y of the state of (c); the component $m_z \approx -m_y$.

the signature of the patterns is a time-independent resistance that increases a square root of the current $R = R_p + \eta(g - g_c)^{1/2}$ when g is negative and goes to zero. The parameter η contains all the information of the applied field, anisotropies, and geometry.

Notice that according to the PDNLS model, Eq. (9) and Eq. (19), the parametric resonance occurs when $\nu \approx 0$ and $\gamma \approx \mu$ or, equivalently, $(g, h_a)_c = -(\beta_z/2, \beta_x + \beta_z/2)$. For a 3-nm-thick material with saturation magnetization similar to cobalt [20], that is, $M_s \simeq 1.4 \times 10^6$ A/m, the critical current density is $J_c = J(g_c) \approx -\beta_z \times 10^9$ A/cm² for a constant $\mathcal{P}(m_x) \approx 1$ polarization function. Since localized states and patterns appear for currents that are fractions of the critical current $|J| \sim 3|J_c|/5$, the smaller the β_z parameters is, the smaller the spin-polarized currents required to observe the parametric phenomenology. Most of our results use $\beta_x = 1/2$ and $\beta_z = 1$;

nevertheless, we have conducted numerical simulations for different values of β_z for β_x in order to achieve the parametric resonance at arbitrary small currents, and the predictions of Eqs. (9) and (19) remain unchanged. The robustness of this parametric phenomenology is a characteristic of systems near their parametric resonance.

V. CONCLUSIONS AND REMARKS

We have shown that nanopillars under the effect of a direct electric current are equivalent to simple rotating magnetic plates. The latter system is characterized by displaying a parametric instability. This equivalence permits us to transfer the known results of the self-organization of parametric

systems to the magnetization dynamics induced by the spin-transfer torque effect. In particular, we have shown that for spin-polarized currents that favor the parallel state the system is governed by the PNDLS equation, and then the magnetization exhibits localized states and patterns both in one and two spatial dimensions. Numerical simulations show a quite good agreement with the analytical predictions.

ACKNOWLEDGMENTS

The authors thank E. Vidal-Henriquez for the critical reading of the manuscript. M.G.C. thanks the financial support of FONDECYT Project No. 1120320. A.O.L. acknowledges the Becas Conicyt 2012, Contract No. 21120878.

-
- [1] *Concepts in Spin Electronics*, edited by S. Maekawa (Oxford University Press, Oxford, 2006).
- [2] J. C. Slonczewski, *J. Magn. Mater. Magn.* **159**, L1 (1996).
- [3] L. Berger, *Phys. Rev. B* **54**, 9353 (1996).
- [4] M. Tsoi, A. G. M. Jansen, J. Bass, W. C. Chiang, M. Seck, V. Tsoi, and P. Wyder, *Phys. Rev. Lett.* **80**, 4281 (1998).
- [5] J. Z. Sun, *J. Magn. Mater. Magn.* **202**, 157 (1999).
- [6] E. B. Myers, D. C. Ralph, J. A. Katine, R. N. Louie, and R. A. Buhrman, *Science* **285**, 867 (1999).
- [7] J. A. Katine, F. J. Albert, R. A. Buhrman, E. B. Myers, and D. C. Ralph, *Phys. Rev. Lett.* **84**, 3149 (2000).
- [8] S. I. Kiselev, J. C. Sankey, I. N. Krivorotov, N. C. Emley, R. J. Schoelkopf, R. A. Buhrman, and D. C. Ralph, *Nature (London)* **425**, 380 (2003).
- [9] S. I. Kiselev, J. C. Sankey, I. N. Krivorotov, N. C. Emley, A. G. F. Garcia, R. A. Buhrman, and D. C. Ralph, *Phys. Rev. B* **72**, 064430 (2005).
- [10] D. C. Ralph and M. D. Stiles, *J. Magn. Mater. Magn.* **320**, 1190 (2008).
- [11] D. V. Berkov and J. Miltat, *J. Magn. Mater. Magn.* **320**, 1238 (2008).
- [12] A. Slavin and V. Tiberkevich, *IEEE Trans. Magn.* **45**, 1875 (2009).
- [13] L. D. Landau and E. M. Lifshitz, *Mechanics*, Course of Theoretical Physics (Pergamon Press, Oxford, 1976), Vol. 1.
- [14] J. W. Miles, *J. Fluid Mech.* **148**, 451 (1984); W. Zhang and J. Viñals, *Phys. Rev. Lett.* **74**, 690 (1995); X. Wang and R. Wei, *Phys. Rev. E* **57**, 2405 (1998); M. G. Clerc, S. Coulibaly, N. Mujica, R. Navarro, and T. Sauma, *Phil. Trans. R. Soc. A* **367**, 3213 (2009).
- [15] B. Denardo, B. Galvin, A. Greenfield, A. Larraza, S. Putterman, and W. Wright, *Phys. Rev. Lett.* **68**, 1730 (1992).
- [16] J. N. Kutz, W. L. Kath, R.-D. Li, and P. Kumar, *Opt. Lett.* **18**, 802 (1993).
- [17] S. Longhi, *Phys. Rev. E* **53**, 5520 (1996).
- [18] I. V. Barashenkov, M. M. Bogdan, and V. I. Korobov, *Europhys. Lett.* **15**, 113 (1991).
- [19] M. G. Clerc, S. Coulibaly, and D. Laroze, *Phys. Rev. E* **77**, 056209 (2008); *Int. J. Bifurcat. Chaos* **19**, 3525 (2009); *Physica D* **239**, 72 (2010); *Europhys. Lett.* **97**, 30006 (2012).
- [20] I. D. Mayergoyz, G. Bertotti, and C. Serpico, *Nonlinear Magnetization Dynamics in Nanosystems* (Elsevier, Oxford, 2009).
- [21] J. Z. Sun, *Phys. Rev. B* **62**, 570 (2000); X. Waintal, E. B. Myers, P. W. Brouwer, and D. C. Ralph, *ibid.* **62**, 12317 (2000); M. D. Stiles and A. Zangwill, *ibid.* **66**, 014407 (2002).
- [22] J. C. Slonczewski, *J. Magn. Mater. Magn.* **247**, 324 (2002).
- [23] J. Xiao, A. Zangwill, and M. D. Stiles, *Phys. Rev. B* **70**, 172405 (2004).
- [24] J. Xiao, A. Zangwill, and M. D. Stiles, *Phys. Rev. B* **72**, 014446 (2005).
- [25] J. Barnas, A. Fert, M. Gmitra, I. Weymann, and V. K. Dugaev, *Phys. Rev. B* **72**, 024426 (2005).
- [26] S.-W. Lee and K.-J. Lee, *IEEE Trans. Magn.* **46**, 2349 (2010).
- [27] W. Kim, S.-W. Lee, and K.-J. Lee, *J. Phys. D* **44**, 384001 (2011).
- [28] M. Lakshmanan, *Phil. Trans. R. Soc. A* **369**, 1280 (2011).
- [29] Z. Li and S. Zhang, *Phys. Rev. B* **68**, 024404 (2003).
- [30] A. A. Andronov and S. E. Khajkin, *Theory of Oscillations* (Dover, London, 1987).
- [31] K. J. Lee, A. Deac, O. Redon, J. P. Nozieres, and B. Dieny, *Nat. Mater.* **3**, 877 (2004).
- [32] M. G. Clerc, S. Coulibaly, M. A. Garcia-Nustes, and Y. Zarate, *Phys. Rev. Lett.* **107**, 254102 (2011).
- [33] D. Anderson, M. Bonnedal, and M. Lisak, *Phys. Fluids* **22**, 1838 (1979).
- [34] I. V. Barashenkov and E. V. Zemlyanaya, *Phys. Rev. E* **83**, 056610 (2011).
- [35] D. Urzagasti, D. Laroze, M. G. Clerc, and H. Pleiner, *Europhys. Lett.* **104**, 40001 (2013).
- [36] P. Couillet, T. Frisch, and G. Sonnino, *Phys. Rev. E* **49**, 2087 (1994).
- [37] A. O. León, M. G. Clerc, and S. Coulibaly, *Phys. Rev. E* **89**, 022908 (2014).